Rock Mechanics: Meeting Society's Challenges and Demands – Eberhardt, Stead & Morrison (eds)
© 2007 Taylor & Francis Group, London, ISBN 978-0-415-44401-9

Effect of confining stress and loading rate on fracture toughness of rocks

T.Y. Ko & J. Kemeny
Department of Mining and Geological Engineering, The University of Arizona, USA

ABSTRACT: In this research, the effect of confining stress and loading rate on the fracture toughness has been investigated. The short beam compression test has been used to estimate the fracture toughness for Flagstaff sandstone. A brief theoretical analysis of the effects of confining stress and loading rate the fracture toughness is presented. This analysis considers changes to the critical fracture process zone size due to confining stress and loading rate. It is found that experimental results agree with the fracture mechanics theory. The mode II fracture toughness is found to increase with increasing confining stress and increasing loading rate.

1 INTRODUCTION

In linear elastic fracture mechanics (LEFM), the stress intensity factor K describes the magnitude of stresses in the crack tip region, the size of the crack tip plastic zone or fracture process zone and its shape, and the strain energy for the crack propagation. Since it is able to correlate the crack propagation and fracture behavior, the stress intensity factor is the most important parameter in LEFM. Cracks will propagate when the stress intensity factor reaches or exceeds a critical stress intensity factor, K_c. The quantity K_c is termed the fracture toughness and is considered to be a material property. Fracture toughness is a quantitative expression of a material resistance to failure when a crack is present. Some particular applications for the fracture toughness of rock are given as follows (ISRM 1988):

(i) a parameter for classification of rock materials.
(ii) an index of the fragmentation process
(iii) a material property in the modeling of rock fragmentation.

According to the loading configurations, there are three basic fracture modes of crack tip deformation, i.e. Mode I (or opening mode), Mode II (or in-plane shearing mode) and Mode III (or out-of-plane shearing mode). Corresponding to the three cracking modes, there are three stress intensity factors known as K_I, K_{II} and K_{III}. Also there are three fracture toughnesses K_{IC}, K_{IIC}, and K_{IIIC} corresponding to the three cracking modes.

Mode II, shear failure is one of the major problems in rock mechanics and rock engineering since it is usually associated with catastrophic failure of geologic structures. One of difficulties in the shear failure studies is producing pure shear failure in laboratory tests. Since most rocks are weaker in tension than compression, not only shear cracks but also tension cracks are produced under shear loading. These tension cracks change the distribution of stresses in the specimen, so the calculated K_{IIC} may be altered by these tension cracks.

In this research, short beam compression (SBC) (Watkins & Liu 1985, Ko et al. 2006) test specimens have been used to investigate the effect of confining stress and loading rate on the Mode II fracture toughness. For a specific slot separation ratio, the SBC specimen gives almost pure shear failure, so it is suitable for determining the Mode II fracture toughness. In this paper, a theoretical analysis of the effects of confining stress and loading rate on the fracture toughness is first presented, followed by a comparison with experimental results.

2 CRACK TIP PROCESS ZONE

2.1 *The fracture process zone (FPZ) in rock*

There must be a region near the crack tip where nonlinear material behavior is predominant. This behavior might be governed by elasto-plastic behavior or microcracking. This region is called the plastic zone in metals or the fracture process zone (FPZ) in geological material such as rock. In rocks, FPZ is due to the initiation and propagation of the microcracks around

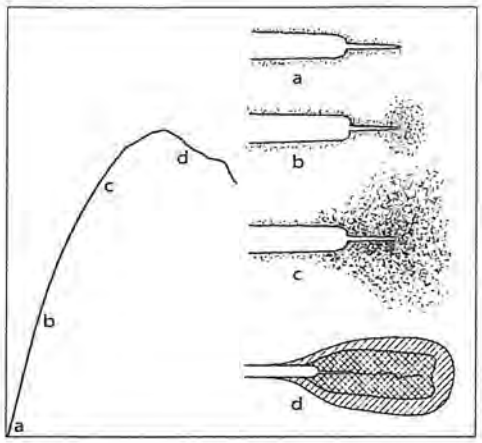

Figure 1. Schematic illustration of four development stages of FPZ in rock. a) initially only a few pre-existing microcracks are present. b) on loading the rock at a low level a few new microcracks are produced. c)with further loading a large number of new microcracks are formed and the FPZ becomes fully developed. d) finally the main crack is extended through the linking the adjacent microcracks.

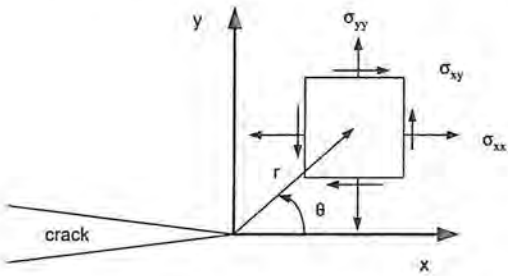

Figure 2. Definition of the coordinate axes ahead of a crack tip.

the crack tip. Hoagland et al. (1973) give a schematic illustration of the four development stages of the FPZ as shown in Figure 1. However, there are no sound theoretical models to describe the shape and size of FPZ and it is often explained using the approximate model for the crack tip plastic zone in metals (Whittaker et al. 1992).

2.2 *Stress components near the crack tip*

For certain cracked configurations subjected to external forces, it is possible to derive closed-form expressions for the stresses in the body, assuming isotropic linear elastic material behavior. If we define a polar coordinate axis with the origin at the crack tip (Fig. 2), it can be shown that the stress field in any linear elastic cracked body is given by (Anderson 1995):

$$\begin{aligned}
\sigma_{xx} &= \frac{K_I}{\sqrt{2\pi r}}\cos\left(\frac{\theta}{2}\right)\left[1-\sin\left(\frac{\theta}{2}\right)\sin\left(\frac{3\theta}{2}\right)\right] \\
&\quad -\frac{K_{II}}{\sqrt{2\pi r}}\sin\left(\frac{\theta}{2}\right)\left[2+\cos\left(\frac{\theta}{2}\right)\cos\left(\frac{3\theta}{2}\right)\right] \\
\sigma_{yy} &= \frac{K_I}{\sqrt{2\pi r}}\cos\left(\frac{\theta}{2}\right)\left[1+\sin\left(\frac{\theta}{2}\right)\sin\left(\frac{3\theta}{2}\right)\right] \\
&\quad +\frac{K_{II}}{\sqrt{2\pi r}}\sin\left(\frac{\theta}{2}\right)\cos\left(\frac{\theta}{2}\right)\cos\left(\frac{3\theta}{2}\right) \\
\tau_{xy} &= \frac{K_I}{\sqrt{2\pi r}}\cos\left(\frac{\theta}{2}\right)\sin\left(\frac{\theta}{2}\right)\sin\left(\frac{3\theta}{2}\right) \\
&\quad +\frac{K_{II}}{\sqrt{2\pi r}}\cos\left(\frac{\theta}{2}\right)\left[1-\sin\left(\frac{\theta}{2}\right)\sin\left(\frac{3\theta}{2}\right)\right] \\
\sigma_{zz} &= 0 \qquad \text{for plane stress} \\
\sigma_{zz} &= \nu(\sigma_{xx}+\sigma_{yy}) \qquad \text{for plane strain}
\end{aligned} \tag{1}$$

The principal stresses in the vicinity of a crack tip can be obtained from the stress components given by equation (1) as follows:

$$\begin{aligned}
\sigma_1 &= \frac{K_I}{\sqrt{2\pi r}}\cos\frac{\theta}{2}\left(1+\sin\frac{\theta}{2}\right) \\
&\quad +\frac{K_{II}}{\sqrt{2\pi r}}\left(-\sin\frac{\theta}{2}+\frac{1}{2}\sqrt{1+3\cos^2\theta}\right) \\
\sigma_2 &= \frac{K_I}{\sqrt{2\pi r}}\cos\frac{\theta}{2}\left(1-\sin\frac{\theta}{2}\right) \\
&\quad +\frac{K_{II}}{\sqrt{2\pi r}}\left(-\sin\frac{\theta}{2}-\frac{1}{2}\sqrt{1+3\cos^2\theta}\right) \\
\sigma_3 &= 0 \qquad \text{for plane stress} \\
\sigma_3 &= \nu(\sigma_1+\sigma_2) \\
&= 2\nu\left(\frac{K_I}{\sqrt{2\pi r}}\cos\frac{\theta}{2}-\frac{K_{II}}{\sqrt{2\pi r}}\sin\frac{\theta}{2}\right) \qquad \text{for plane strain}
\end{aligned} \tag{2}$$

2.3 *FPZ size and shape*

Schmidt (1980) proposed using the maximum normal stress criterion to show the shape and size of the FPZ. When the local maximum principal stress around the crack tip reaches the ultimate tensile strength of the rock, an FPZ occurs. For this case, the maximum normal stress criterion can be simply stated as:

$$\sigma_1 = \sigma_t \tag{3}$$

where σt is the tensile stress and tensile stresses are taken as positive.

Combining Equations 3 and 2 and solving for r under mode I loading gives:

$$r(\theta) = \frac{1}{2\pi}\left(\frac{K_I}{\sigma_t}\right)\cos^2\frac{\theta}{2}\left(1+\sin\frac{\theta}{2}\right)^2 \tag{4}$$

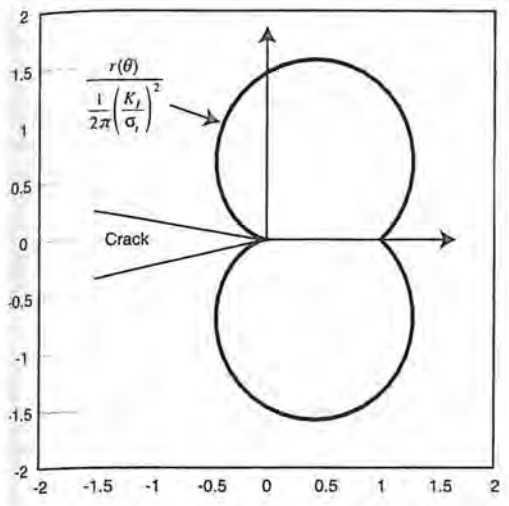

Figure 3. Normalized FPZ shape for mode I loading. Both the x and y axis are distance normalized by Equation 6.

and similarly solving for r under mode II loading gives:

$$r(\theta)=\frac{1}{2\pi}\left(\frac{K_{II}}{\sigma_t}\right)^2\left[-\sin\frac{\theta}{2}+\frac{1}{2}\sqrt{1+3\cos^2\theta}\right]^2 \qquad (5)$$

From Equations 4 and 5, it follows that the characteristic FPZ size when $\theta=0°$ is given by:

$$r(0°)=\frac{1}{2\pi}\left(\frac{K_I}{\sigma^t}\right)^2 \quad \text{for mode I loading} \qquad (6)$$

and

$$r(0°)=\frac{1}{2\pi}\left(\frac{K_{II}}{\sigma^t}\right)^2 \quad \text{for mode II loading} \qquad (7)$$

The normalized shapes of the FPZ under modes I and II loading are schematically illustrated in Figures 3 and 4.

Figure 3 shows that the shape of the FPZ in mode I is symmetric about the x-axis. This follows from the fact that for mode I the loading and also the stress distribution is symmetric about the axis of the crack. In the case of mode II, loading is asymmetrical about the x-axis, so the shape of the FPZ is asymmetrical as well.

At the onset of crack propagation, K reaches K_C and $r(\theta)$ attains a critical value, $r_c(\theta)$, which is also a material property.

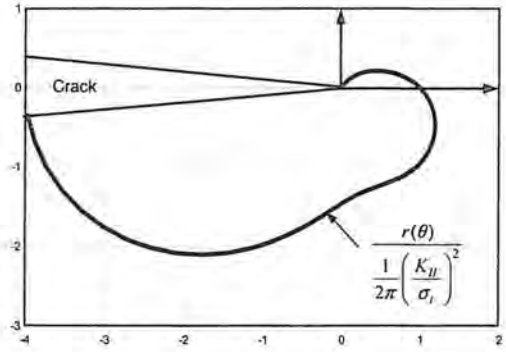

Figure 4. Normalized FPZ shape for mode II loading. Both the x and y axis are distance normalized by Equation 7.

3 EFFECT OF CONFINING STRESS

Without invoking LEFM, it is reasonable to assume that fracture toughness increases with increasing confining stress. This follows since increasing the confining stress causes the closure of pre-existing microcracks, and reducing the microcrack density increases rock strength. As shown in what follows, a simple analysis based on the LEFM provides an analytical solution for the effect of confining stress on fracture toughness.

Schmidt (1980) analyzed the effect of confining stress on the shape and size of the FPZ. In the case of mode I loading, adding a uniform confining stress p to the crack tip principal stresses and it gives:

$$\sigma_1=\frac{K_I}{\sqrt{2\pi r}}\cos\frac{\theta}{2}\left(1+\sin\frac{\theta}{2}\right)-p$$
$$\sigma_2=\frac{K_I}{\sqrt{2\pi r}}\cos\frac{\theta}{2}\left(1-\sin\frac{\theta}{2}\right)-p \qquad (8)$$

Substituting Equation 8 into Equation 3 and solving for $r(\theta)$ gives the size of the FPZ as follows:

$$r(\theta)=\frac{1}{2\pi}\left(\frac{K_I}{\sigma_t+p}\right)^2\cos^2\frac{\theta}{2}\left(1+\sin\frac{\theta}{2}\right)^2 \qquad (9)$$

In order to maintain a constant value of $r_c(\theta)$ at the moment of crack propagation, the ratio of K_{IC} without confining stress to σ_t must be equal to the ratio of K_{IC} with confining stress to $\sigma_t + p$ (Whittaker et al. 1992).

Therefore confining stress and fracture toughness should be related as follows:

$$\frac{K_{IC}(o)}{\sigma_t}=\frac{K_{IC}(p)}{\sigma_t+p}$$

or (10)

$$K_{IC}(p)=(1+\frac{p}{\sigma_t})K_{IC}(o)$$

where $K_{IC(o)}$ is K_{IC} without confining stress and $K_{IC(p)}$ is K_{IC} with confining stress.

Table 1. The mechanical properties of Flagstaff sandstone (σ_c: uniaxial compressive strength, σ_t: tensile strength, E: Young's modulus, v: Poisson's ratio, ϕ: internal friction angle, c: cohesion).

σ_c (MPa)	σ_t (MPa)	E (GPa)	v	ϕ(°)	c (MPa)
116.83	6.38	24.3	0.357	52.04	20.42

Similarly for the case of mode II,

$$K_{IIC}(p)=(1+\frac{p}{\sigma_t})K_{IIC}(o) \tag{11}$$

4 EFFECT OF LOADING RATE

It has been frequently observed that the strength and deformation properties of rock increase with increasing loading rate (Hudson & Harrison 1997).

Since fracture toughness is proportional to the applied strength at failure, one can assume that fracture toughness also increases with increasing loading rate. This phenomenon also can be explained with the LEFM concepts.

At a low loading rate, the FPZ develops due to the subcritical crack growth and critical crack growth under the the applied loading. But at a high loading rate, the FPZ develops without significant subcritical crack growth. A rock specimen must have a constant critical FPZ size at failure, therefore in the case of a high loading rate, it needs a higher applied load. Consequently, a higher value of fracture toughness is measured.

5 EXPERIMENTAL RESULTS

Flagstaff sandstone was used to measure the fracture toughness. The mechanical properties are given in Table 1.

5.1 *Specimen geometry and loading*

The test specimen has a length of $W = 101.6$ mm (4 in), a width of $L = 50.8$ mm (2 in) and a thickness of $B = 25.4$ mm (1 in). Two equal and opposite pre-existing slots, which have a depth of $a=L/2$, and slot separation of $c = 20.32$ mm (0.8 in), are cut perpendicular at the central part of specimen. An axial compressive load was applied on the end surfaces of the specimen. For the loading rate test, loading rates ranging from 0.01 to 5 MPa/s were used. For the test with a confining stress, lateral confinement was applied to the specimen from 1 to 10 MPa with the loading rate of 0.1 MPa/s. The test specimen and schematic illustration of the testing apparatus are illustrated in Figure 5.

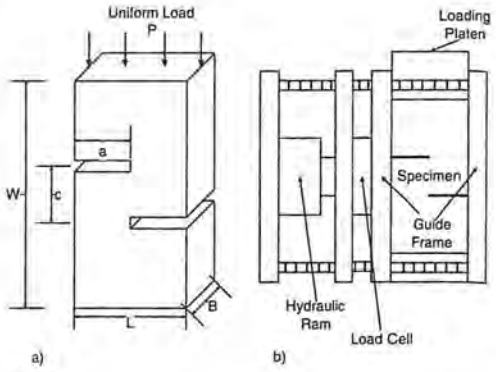

Figure 5. Short beam compression test: a) specimen geometry; b) testing apparatus.

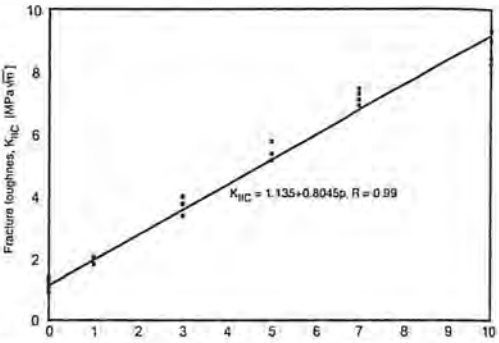

Figure 6. The variation of the fracture toughness with respect to the confining stress.

Ko & Kemeny (2006) developed the stress intensity factor for the SBC specimen using finite element technique and is given as follows:

$$K_{II}=(0.15+0.54\frac{c}{W})\frac{P}{Bc}\sqrt{\pi a} \tag{12}$$

where P is the applied load.

5.2 *Influence of confining stress on fracture toughness*

The average fracture toughness without confining stress is 1.135 MPa$\sqrt{m}$ with a standard deviation of 0.178 MPa$\sqrt{m}$. The variation of fracture toughness for different confining stresses is presented in Figure 6.

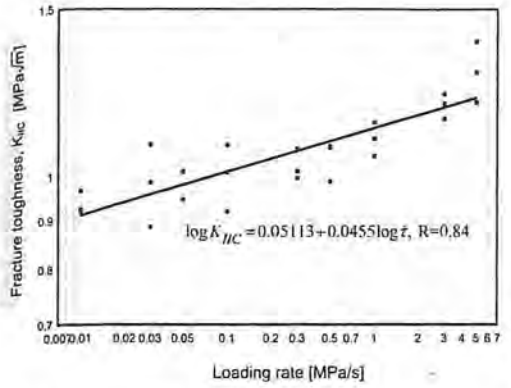

Figure 7. The variation of the fracture toughness with respect to the loading rate.

A total of 25 tests were conducted. An approximate empirical relationship between fracture toughness and confining stress can be expressed as:

$$K_{IIC(p)} = (1 + 0.709p) K_{IIC(o)} \quad (13)$$

The experimental results show a similar variation of fracture toughness increase as that with Equation 11.

5.3 *Influence of loading rate on fracture toughness*

The experimental results are presented in Figure 7, where fracture toughness is plotted as a function of loading rate using a log-log scale. A total of 26 tests were conducted, with about 3 tests conducted at each loading rate. Even though there is a scatter in the results, there is a definite trend of increasing fracture toughness with increasing loading rate. The solid line in Figure 7 shows the best-fit regression line based on the log fracture toughness versus log loading late data. This empirical relationship between fracture toughness and loading rate is given as follows:

$$\log K_{II} = 0.05113 + 0.04555 \log \dot{\tau} \quad (14)$$

The experimental results agree with the theory as stated earlier.

6 CONCLUSIONS

Fracture toughness is a quantitative expression of a material's resistance to failure when a crack is present and it is an important parameter in LEFM. In this research, the effects of confining stress and loading rate on the fracture toughness were investigated. The short beam compression test has been used to estimate the fracture toughness for Flagstaff sandstone.

A brief theoretical analysis of the effects of confining stress and loading rate on the fracture toughness has been presented. It has been found that experimental results agree with theory. The mode II fracture toughness has been found to increase with increasing confining stress and increasing loading rate.

ACKNOWLEDGEMENT

This work supported by University of Arizona NIOSH contract R01 OH007739.

REFERENCES

Anderson, T.L. 1995. *Fracture Mechanics*. CRC Press.

Hoagland, R.G., Hahn, G.T. & Rosenfield, A.R. 1973. Influence of microstructure on fracture propagation in rock. *Rock Mechanics* 5: 77–106.

Hudson, J.A. & Harrison, J.P. 1997. *Engineering Rock Mechanics*. Elsevier Science.

ISRM 1988. Suggested methods for determining the fracture toughness of rock. *Int. J. Rock Mech. Min. Sci. & Geomech. Abstr.* 25(2): 71–96.

Ko, T.Y. & Kemeny, J. 2006. Determination of mode II stress intensity factor using short beam compression test. In *Proceedings of the 4th Asian Rock Mechanics Symposium, Singapore*. CD-Rom.

Ko, T.Y., Kemeny, J. & Lee, J.S. 2006. Mode II subcritical crack growth parameters for sandstone. In *Proceedings of the 41st U.S. Rock Mechanics Symposium, Golden*. CD-Rom

Schmidt, R.A. 1980. A microcrack model and its significance to hydrulic fracturing and fracture toughness testing. In *Proceedings of the 21st U.S. Rock Mechanics Symposium*, pp. 581–590

Watkins, J. & Liu, K.L.W. 1985.A finite element study of the short beam test specimen under mode II loading. *International Journal of Cement Composites and Lightweight Concrete* 7(1): 39–47.

Whittaker, B.N., Singh, R.N. & Sun, G.1992. *Rock Fracture Mechanics: Principles, Design and Applications*. Elsevier Publishing Company.